PCCP

Accepted Manuscript

ROYAL SOCIETY OF CHEMISTRY

www.rsc.org/pccp

PCCP

PAPER

Characterization of the phase behaviour of a novel polymerizable lyotropic ionic liquid crystal

Received 00th January 20xx,
Accepted 00th January 20xx

DOI: 10.1039/x0xx00000x

www.rsc.org/

Nicolas. Goujon,[a] Maria. Forsyth,[ab] Ludovic. F. Dumée,[a] Gary. Bryant,[c] and Nolene. Byrne*[a]

The development of new polymerizable lyotropic liquid crystals (LLCs) utilizing charged amphiphilic molecules such as those based on long chain imidazolium compounds, is a relatively new design direction for producing robust membranes with controllable nano-structures. Here we have developed a novel polymerizable ionic liquid based LLC, 1-hexadecyl-3-methylimidazolium acrylate (C_{16}mimAcr), where the acrylate anion acts as the polymerizable moiety. The phase behaviour of the C_{16}mimAcr upon the addition of water was characterized using small and wide angle X-ray scatterings, differential scanning calorimetry and polarized optical microscopy. We compare the phase behaviour of this new polymerizable LLC to that of the well known LLC chloride analogue, 1-hexadecyl-3-methylimidazolium chloride (C_{16}mimCl). We find that the C_{16}mimAcr system has a more complex phase behaviour compared to the C_{16}mimCl system. Additional lyotropic liquid crystalline mesophases such as hexagonal phase (H_1) and discontinuous cubic phase (I_1) are observed at 20 °C for the acrylate system at 50 and 65 wt. % water respectively. The appearance of the hexagonal phase (H_1) and discontinuous cubic phase (I_1) for the acrylate system is likely due to the strong hydrating nature of the acrylate anion, which increases the head group area. The formation of these additional mesophases seen for the acrylate system, especially the hexagonal phase (H_1), coupled with the polymerization functionality offers great potential in the design of advanced membrane materials with selective and anisotropic transport properties.

Introduction

Lyotropic liquid crystals (LLCs) have attracted a great deal of interest in recent years due to their potential application in drug delivery, energy devices, membrane separations and as templating substrates.[1-5] Lyotropic liquid crystalline phases are formed by the spontaneous self-assembly of amphiphilic molecules with the addition of a co-solvent, typically water, alcohol or glycerol.[6-10] A wide variety of mesophases exist including lamellar, hexagonal (normal & inverted), discontinuous cubic (*Im3m, Fm3m, Pm3n, Fd3m*) and bicontinuous cubic (*Im3n, Pn3m, Ia3d*).[9, 11-14] These architectures display exceptional properties such as bimodal pore size distribution (i.e. discontinuous cubic phase) or anisotropic transport properties (i.e. hexagonal phase), making them excellent candidates for the development of advanced nanoporous materials.[2, 15]

Among the large diversity of LLC molecules already reported in the literature, one of the most important classes is charged surfactants.[13, 16-20] This class has been intensely studied due to the ease of tailoring the surfactant chemistry (including anion type, cation type or alkyl chain length) to target specific application needs. Imidazolium based ionic liquids bearing long alkyl chains (i.e. carbon number larger than 8) belong to the charged surfactant class of materials and have shown typical LLC behaviour upon addition of a co-solvent and as a function of temperature.[19, 21-24]

A major drawback in the use of LLCs for the design of well-defined nanostructured systems for targeted material applications, such as membrane separation, is the poor mechanical properties of the LLC, which is strongly related to the nanostructure stability and orientation. Since most LLC systems reported typically have a gel-like physical state they therefore do not meet the mechanical requirements of many material applications.[25] Additionally, the mesophases formed by these LLC systems are extremely sensitive to the co-solvent concentrations as well as temperature, making these materials again not sustainable for many applications where extreme conditions are used.[25, 26] A solution to this lies in the development of photo-polymerized LLC system whereby long range order could be maintained after UV-exposure. Successful photo-polymerization of traditional LLC/water systems has already been reported using different crosslinking polymers, resulting in highly ordered porous polymers.[3, 27-30] The nanostructure observed in these polymers is significantly impacted by the type of mesophase formed by the LLC

[a] *Institute for Frontier Materials, Deakin University, Waurn Ponds, Victoria 3216, Australia.*
E-mail: nolene.byrne@deakin.edu.au
[b] *ARC Centre of Excellence for Electromaterials Science (ACES), Australia.*
[c] *Centre for Molecular and Nanoscale Physics, School of Applied Sciences, RMIT University, GPO Box 2476, Melbourne, Victoria 3001, Australia.*
Electronic Supplementary Information (ESI) available: Details on the phase assignment using the SAXS data as well as additional SAXS data of both ionic liquids/water systems. See DOI: 10.1039/x0xx00000x

systems.[27] In this approach, LLC systems are used as a structure template and then they are removed post-polymerization, leading to the formation of nanoscale porosity. However, this approach is not favoured for the design of nanostructured and advanced materials, where the LLC system is only used as a scaffold for the incorporation of host molecules or particles and not as a structure template for the design of highly ordered porous polymers.[3, 31, 32] A viable solution to this problem is to covalently bond the amphiphilic molecules with the crosslinking polymer in order to make the nanostructure formed by the LLC system part of the resulting nanostructured polymer.[2, 25, 31, 32] More recently, a lot of attention in the area of LLC design and characterization has focused on the conception of LLCs with polymerizable moieties.[4, 18, 31-33] The design of polymerizable LLCs can be achieved by utilizing a reactive amphiphilic molecule, and it is conceivable that the class of charged surfactants, i.e. ionic liquid based, could be utilized in the development of new polymerizable LLCs by the incorporation of a polymerizable moiety. The ease of tailoring the chemistry of imidazolium based ionic liquids makes them an excellent candidate for the incorporation of polymerizable moieties.[2, 18, 31, 32, 34]

A greater knowledge of the impact of the type of polymerizable moieties incorporated, as well as their locations on the amphiphilic molecule, on the formation of liquid crystalline phase is still required for the development of advanced nanostructured materials. Here we have developed a novel polymerizable ionic liquid based LLC, 1-hexadecyl-3-methylimidazolium acrylate (C_{16}mimAcr), where the acrylate anion acts as a polymerizable moiety. Using a combination of small and wide angle X-ray scatterings (SAXS and WAXS), polarized optical microscopy (POM) as well as differential scanning calorimetry (DSC) techniques, the phase behaviour and the phase transition temperature of the C_{16}mimAcr were characterized as a function of water content. These results have been compared with the well known chloride analogue, 1-hexadecyl-3-methylimidazolium chloride (C_{16}mimCl) in order to understand the impact of the incorporation of the polymerizable moiety (i.e. acrylate anion) on the formation of the liquid crystalline phase. Finally, the binary aqueous phase diagrams of the C_{16}mimAcr and C_{16}mimCl at 20 °C are presented and compared. This study aims to give highlights on the design of a polymerizable ionic liquid based LLC and more importantly on the impact of a polymerizable moiety on the phase behaviour and phase transition temperature as function water content. A better understanding of these effects is still required for the development of more efficient advanced nanostructured materials with targeted nanostructure and transport properties.

Experimental

Chemicals and Materials

1-methylimidazole (99 %), acrylic acid (99 %) and Amberlyst-26 OH form were purchased from Sigma-Aldrich and used as received. 1-chlorohexadecane (97 %) was purchased from Alfa Aesar and used as received. 1.5 mm outer diameter special glass 10 capillaries were purchased from Hampton Research Corporation.

Ionic liquid synthesis

1-hexadecyl-3-methyl-imidazolium chloride (C_{16}mimCl)

1-hexadecyl-3-methyl-imidazolium chloride (C_{16}mimCl) was synthesized according to the following procedure. In a 250 mL round bottom flask equipped with a reflux condenser, 1-methylimidazole (11.96 g, 0.1458 mol) and 1-chlorohexadecane (43.13 g, 0.160 mol) were added simultaneously. Then, the mixture was stirred at 80 °C for 72 hours under a nitrogen atmosphere resulting in a slightly yellow solid. Then, the product has been purified by recrystallization in ethyl acetate, two times. Finally, the pure C_{16}mimCl was dried under high vacuum for several hours, resulting in a white powder product.

1H-NMR(500MHz; DMSO-d6, ppm): 9.49 (s, 1H), 7.86 (s,1H), 7.80 (s,1H), 4.18 (t,2H), 3.87 (s,3H), 1.75 (m,2H), 1.20 (m, 26H), 0.82 (t,3H)

1-hexadecyl-3-methylimidazolium Acrylate (C_{16}mimAcr)

Firstly, 300 g of ion exchange resin (Amberlyst-26 OH form) was loaded with the desired acrylate anion using a 10 wt.% acrylic acid solution (1000 ml). The resin was then washed with an abundant amount of Milli-Q water in order to remove the unreacted acrylic acid residue. 30.03 g of 1-hexadecyl-3-methyl-imidazolium chloride was dissolved in 100 ml of Milli-Q water and the aqueous solution of ionic liquid was flushed through the column 10 times. The acrylate based ionic liquid was concentrated and dried under high vacuum resulting in a slightly gel-like material. Then, the product was purified by recrystallization in ethyl acetate, two times. Finally, the pure C_{16}mimAcr was dried under high vacuum for several hours, resulting in a white powder product.

1H-NMR(500MHz; DMSO-d6, ppm): 9.71 (s, 1H), 7.84 (s,1H), 7.77 (s,1H), 5.97-5.92 (dd, 1H), 5.69-5.66 (dd,1H), 5.13-5.10 (dd,1H), 4.17 (t,2H), 3.87 (s,3H), 1.75 (m,2H), 1.21 (m, 26H), 0.82 (t,3H)

Lyotropic liquid crystalline phase preparation

The lyotropic liquid crystalline phases were prepared by weighing the appropriate amounts of ionic liquid and Milli-Q water. The samples were then sonicated for several hours as well as gently heated and mixed using a vortex agitator.

SAXS and WAXS

Small-angle-X-ray scattering (SAXS) and Wide-angle-X-ray scattering (WAXS) measurements were recorded with a microcalix SAXS system (Bruker) using Cu Kα radiation (50 KV, 10 mA). The samples were placed into a 1.5 mm outer diameter capillary (special glass #10) and then the capillary were sealed with an epoxy resin. Measurements were carried out under vacuum at 20 °C with exposure times of 600

seconds. The program Fit2D was used to extract the 1D-SAXS profile (i.e. Intensity vs. scattering vector, $q = (4\pi Sin\theta)/\lambda$), both presented in logarithmic scale. The spectra were not corrected with the scattering of an empty capillary since the background subtraction produced negative data. Therefore, the broad peak observed at 0.4 $Å^{-1}$ is due the kapton windows of the instrument.

DSC

Differential Scanning Calorimetry (TA Instrument-Q200) was used to determine the phase transitions of the different systems. The samples were accurately weighted into a standard aluminium pans. The weigh of the pans containing the sample were measured before and after the DSC measurement to determine eventual weight loss, which was attributed to water loss.

For the ionic liquid/ water mixtures, the samples were heated from 203.15 K to 353.15 K and then cooled down from 353.15 K to 203.15 K at a rate of 10 $K.min^{-1}$. For the pure ionic liquid, although a similar heating/cooling sequence was used, the sample was heated up to 423.15 K.

POM

The textures of lyotropic liquid crystalline phases were obtained by a polarized optical microscope (Nikon Eclipse 80i), equipped with a heating stage (Linkam Scientific LTS350) and a charge-coupled device camera (Nikon DS-U1). The POM images were acquired under crossed polarizers and using a ¼ lambda plate. The use of the ¼ lambda plate has the consequence of altering the polarization state of the light, resulting in the appearance of green colour instead of black for isotropic sample.

Results and discussion

DSC

C_{16}mimCl/water system.

Figure 1a shows the DSC profiles of C_{16}mimCl as a function of water content. The lowest water content measured here is 4.8 wt.% since the complete removal of water from this system was very difficult. A single endothermic transition is observed at 69.4 °C, this transition represents the crystal-mesophase transition.[35, 36] As more water is added to the system, multiple endothermic transitions are observed indicating the melting of various crystal phases into a SmA_2 phase, each with slightly different hydration levels. The complex endothermic events observed between 10 °C and 50 °C for the sample containing 20 wt.% water (green curve, Figure 1a.) simplifies significantly into a single endothermic event observed at 22 °C for the sample with 30 wt.% water. At 30 wt.% water content, the physical state of the sample changes from a waxy-like material to a gel. As such the endothermic peak now represents a lamellar gel phase to micellar phase transformation[26] as previously suggested by Wu *et. al.* At higher water contents (i.e. 65 wt.% and 70 wt.% water) the endothermic event, which appears at 15 °C, represents melting into a liquid phase. The endothermic transition at 0 °C present from 30 wt.% water represents a lamellar crystalline to a lamellar gel phase transformation, as suggested by Wu *et. al.*,[26] which becomes sharper as the water content is increased.

As previously stated, drying the C_{16}mimCl to lower than 4.8 wt.% water was very difficult, therefore repeated DSC scans of C_{16}mimCl containing initially 4.8 wt.% water were performed, Figure 1c. With each scan the water is being removed from the system, as verified by a weight loss measurement. Approximately, 1.28 wt.% lost is observed after the DSC measurement. As can be seen, the C_{16}mimCl at 4.8 wt.% water exhibits only one endothermic transition at 69.4 °C representing the crystal-mesophase transition of the hydrated crystal phase [35, 36]. With subsequent scans the appearance of a second endothermic transition at 51.4 °C is observed, suggesting that the system has segregated into two distinct crystal phases with different water contents.

C16mimAcr/water system.

Figure 1b shows the DSC profiles of the C_{16}mimAcr as a function of water content. The lowest water content measured here is 4.9 wt.% (again complete removal of water from this system was very difficult). A broad endothermic event at 45 °C is observed likely representing a crystal-mesophase transition. This endothermic transition has a clear higher temperature shoulder present, which represents the melting of multiple crystal phases into a SmA_2 phase with different hydration levels. Similar to the observations with C_{16}mimCl, as water is added multiple crystal phases become present, however the width of the endothermic peak is narrower in the acrylate system compared with the chloride system suggesting a more homogenous dispersion of phases. At 30 wt.% water (pink curve, Figure 1b) the system is a gel at room temperature similar to the C_{16}mimCl. A notable difference between the acrylate and the chloride system is that, with water increasing to the highest water content measured here, the dominance of one endothermic peak is observed (as opposed to two in the 70 wt.% water in the C_{16}mimCl system), this suggests that water is more evenly incorporated into the system.

Again repeat DSC scans were performed on the lowest water content sample for the acrylate system and shown in Figure 1d. Here the crystal-mesophase transition was lowered by 7 °C with a single and clearly sharper endothermic transition being observed as a result of the multiple scans, approximately 2.75 wt.% water is lost. Again, this suggests a better incorporation of the water into the acrylate based system when compared to the chloride system, likely due to the difference in the geometry and the hydrogen bond abilities of the two anions.

SAXS and WAXS

C_{16}mimCl/water system.

Figure 2 shows the complete SAXS profiles of C_{16}mimCl as a function of water content highlighting the phase changes as well as a schematic representation of the phase present. The structure of the C_{16}mimCl with 4.8 wt.% water is identified as a

lamellar phase (L_α) with the first diffraction peak appearing at q = 0.111 $Å^{-1}$, corresponding to a repeat distance d = 2π/q = 56.5 Å. This d value corresponds to approximately twice the molecular length of the fully extended cation (i.e. ~ 50 Å in absence of the chloride anion).[26] In practice the repeat distance is equal to the thickness of the bilayer plus the thickness of the water layer, so at 4.8 wt.% water, the water layer will be a small fraction of this distance. The formation of this extended bilayer (i.e. alkyl chains are packed end to end) has been previously observed by Bradley *et. al* and Doward *et. al* for this system. [35, 36] As the water content increases to 10 wt.%, the water now forms a substantial layer between the bilayers, but the repeat distance is reduced significantly to 26.2 Å. This can only occur if the extended bilayer conformation disappears and the system adopts an interdigitated bilayer conformation.[35, 36] As the water content increased from 10 wt.% to 30 % wt. this repeat distance d increases from 26.2 Å to 40.1 Å. Additionally, for the 10 wt.% and 20 wt.% water samples, the SAXS profiles show an extra low q peak, which may correspond to an additional lamellar phase in an interdigitated bilayer conformation for each concentration.

As the water increases from 40 wt.% water to 60 wt.% water, a biphasic system is observed, as suggested by the appearance of an extra broad diffraction peak centred at q = ~ 0.11 $Å^{-1}$ (Figure 2). This diffraction peak corresponds to an inter-micelle interference peak, indicating the correlation lengths of pair distribution functions of micelles, ξ_c = 57 Å (i.e. q = 2π/ξ_c).[20, 26] The coexistence of the lamellar phase and the micellar phase (L_1) is observed up to 60 wt.% water, beyond this, i.e. 70 wt.% water, only a micellar phase is observed. Interestingly, a phase separation occurs for the C_{16}mimCl containing 60 wt.% water, resulting in the formation of a gel phase and a liquid phase (See Figure 2). The SAXS pattern of the gel phase suggests the coexistence of the lamellar phase and the micellar phase, while the liquid phase corresponds only to a micellar phase.

The nature of the physical states and changes from crystalline to gel-like or fluid were assessed by WAXS. The WAXS profiles of the C_{16}mimCl as a function of water concentration are shown in Figure 3. Figure 3a shows the samples with 4.8 wt.% to 30 wt.% water. As expected the sample with low water is a highly ordered well packed crystal.[10, 26, 37] This configuration remains with water loading up to 20 wt.%. At 20 wt.% the system start to undergo a crystal-mesophase transition at 20°C as suggested by the DSC data. At 30 wt.% water, the WAXS profile changes drastically as does the physical state of the sample, going from a solid to a gel, with the spectra showing only a single peak observed at q = 1.51 $Å^{-1}$ corresponding to a repeat distance d = 4.1 Å. This peak represents the carbon-carbon packing of the alkyl chains; it can be seen that as water content is increased, Figure 3b, this peak intensifies and becomes sharper, indicating a better packing of the alkyl chains in these gel-like materials. At water concentrations above 50 wt.% the peak intensity gradually disappears and the presence of a more diffuse peak centred at q = ~ 1.46 $Å^{-1}$ is observed as shown in Figure 3c. This reflects a looser packing of the alkyl chains, characteristic of a fluid state.[10, 26, 37]

All the peak assignments as well as the lattice parameter, a, for the C_{16}mimCl/water system are listed in Supporting Information.

C_{16}mimAcr/water system.

Figure 4 shows the complete SAXS profiles of the C_{16}mimAcr as a function of water content highlighting the phase changes as well as a schematic representation of the phase present. The SAXS profile of the sample containing 4.9 wt.% water suggests that two main lamellar phases can be identified $L_{\alpha1}$ and $L_{\alpha2}$ representing a relatively "dry" and wet phase where $L_{\alpha1}$, q_1 (100) = 0.225 $Å^{-1}$, corresponding to a repeat distance d =2π/q = 34.2 Å and $L_{\alpha2}$, q_1 (100) = 0.183 $Å^{-1}$ corresponding to a repeat distance d =2π/q = 27.9 Å. The repeat distance of the two lamellar phases suggests the formation of an interdigitated bilayer configuration. For the samples containing between 10 wt.% and 20 wt.% water, the SAXS profile shows multiple lamellar phases in an interdigitated bilayer structure with a gradual increase in the d spacing, likely due to an increase of the water layer thickness.

A change from lamellar to hexagonal phase (H_1) is observed with increasing water content for samples containing 30 wt.% and 40 wt.% water, however, both lamellar and hexagonal phases are present. The repeat distance d for the lamellar phase and hexagonal phase are approximately 40.0 Å and 42.4 Å respectively. For the sample containing 50 wt.% water, only the hexagonal phase is observed, showing a characteristic hexagonal pattern: q_1 (100) : q_2 (110) : q_3 (200) : q_4 (210) = 1:√3:√4:√7 (Figure 4). The d spacing for the 50 wt.% hexagonal phase has increased to 46.5 Å indicating a looser packing of the micellar cylinders.[9]

At around 60-65 wt.% water, the formation of a discontinuous cubic phase (I_1) is observed, as evidenced by the SAXS profiles in Figure 4. Discontinuous cubic phases have been reported to be located between the micellar phase (L_1) and hexagonal phase (H_1).[9, 11-13, 16, 38, 39] The I_1 present in the C_{16}mimAcr/water system could be properly indexed as a *Pm3n* lattice with up to 13 identified reflection peaks. The *Pm3n* space group consists of two spherical and six disc-shaped micelles per unit as proposed by Charvolin and Sadoc [9, 13, 17, 40, 41] The unit cell parameter, a, for the I_1 phase is determined to be equal to 117 Å for the sample containing 65 wt.% water.

Past the I_1 phase, the formation of a micellar phase (L_1) is observed as suggested by the appearance of an inter-micelle interference peak centred at q = ~ 0.11 $Å^{-1}$. This indicates the correlation lengths of pair distribution function of micelles, ξ_c = 57 Å (i.e. q = 2π/ξ_c).[20, 26]

All the peak assignments as well as the lattice parameter, a, for the C_{16}mimAcr/water system are listed in Supporting Information.

Again, the physical state of the C_{16}mimAcr system as a function of water was assessed by WAXS. The WAXS profiles of the C_{16}mimAcr at 20 °C containing 4.9 wt.% water to 30 wt.% are shown in Figure 5a. For the sample containing 4.9 wt.% water,

it is a highly ordered crystal (or perhaps two highly ordered crystals) as suggested by the WAXS data (Figure 5a).[10, 26, 37] For the C_{16}mimAcr system the highly ordered arrangement is present up to 10 wt.% water. At 20 to 30 wt.% water, the WAXS profiles still show some reflection peaks, which can be indexed as part of the lamellar phase remaining. However the peak centred at q = ~ 1.39 $Å^{-1}$ corresponds to the carbon-carbon packing information in the alkyl chains, giving a repeat distance d = ~ 4.5 Å.[10, 26, 37] This carbon-carbon packing could be attributed to the lamellar phase as suggested by the disappearance of this peak when the hexagonal phase is only present (i.e. 50 wt.% water), as be seen in Figure 5b.

Around 40-65 wt.%, the presence of a more diffuse peak centred at q = ~ 1.4 $Å^{-1}$ is observed, corresponding to a looser packing of the alkyl chains.[10, 26, 37] This peak progressively vanishes beyond 70 wt.% water, which is consistent with the decline of the intermicelle interference peak in the SAXS region.

Polarized optical microscopy has been used as a complementary technique to identify the mesophases present in the C_{16}mimAcr/water system. Figure 6 shows the POM images of the C_{16}mimAcr at 20 wt.% (a), 40 wt.% (b) and 60 wt.% (c) at room temperature. As can be seen in Figure 6a, a characteristic texture of a lamellar phase is observed for the sample containing 20 wt.% water.[19, 21, 22, 42, 43] The optical texture of the C_{16}mimAcr at 40 wt.% water (Figure 6b) is distinctive of a hexagonal phase (H_1).[14, 21, 22, 42, 43] The POM image of the sample with 60 wt.% water (Figure 6c) shows no birefringence, consistent with the formation of a discontinuous cubic phase (I_1) as suggested by the SAXS data.[9]

Comparison between between C16mimCl/water and C16mimAcr/water system

From the SAXS and WAXS data taken at 20 °C, the C_{16}mimAcr/water system shows a more complex phase behaviour compared to the chloride system. At low water content (i.e. below 20 wt.% water), the crystal packing arrangement of the C_{16}mimCl is less disrupted by water addition compared to the C_{16}mimAcr, as suggested by the WAXS data, which showed the existence of a highly ordered well packed crystal being maintained up to water concentrations of 20 wt.% for the C_{16}mimCl. On the other hand, the crystal packing arrangement was maintained in the acrylate system up to a water content of 10 wt.%. These results are consistent with the DSC observations that show that the shift to higher temperature of the crystal-mesophase transition is more pronounced for the C_{16}mimCl compared to the C_{16}mimAcr. This is likely due to the differences in the geometry of the two anions i.e the bulky shape of the acrylate anion. In addition to the differences in anion geometry, the binding between the anion and the water is also different with the water weakly binding with the chloride compared to acrylate.[44] Previous studies have shown that water molecules are favourable to form hydrogen bond with the proton of the imidazolium ring (i.e. proton H_2, located between the two nitrogen atom) as well as with the anion and therefore breaks up the imidazolium ring –anion hydrogen bond and the ring–ring assembly.[45-48]

Figure 7 shows the phase diagrams as a function of water content for the two ionic liquids systems. As the water content increases, the C_{16}mimCl system undergoes the following phase transitions, lamellar gel (L_α) phase to a micellar phase (L_1). While the C_{16}mimAcr system experiences a more complex phase transition behaviour, going from a lamellar gel phase (L_α), followed by the formation of a Hexagonal phase (H_1), then of a discontinuous cubic phase (I_1) and finally of a micellar phase (L_1). It is well known that the counterion plays an important role in the self-assembly of a cationic surfactant structures, since changing the binding properties of the couterion impacts the effective head group area.[44] The appearance of the hexagonal (H_1) and discontinuous cubic phase (I_1) for the acrylate system again highlights how the different anion geometries impact the systems structure and how the water molecules are intercalated in the system. Again, the binding between the anion and the water is also different with the water weakly binding with the chloride compared to acrylate leading to a increase of the head group area due to the intercalation of water molecules between the imidazolium ring and the anion.[44 45, 46, 49] These results are consistent with the greater temperature shift observed for the $Lamellar_{gel}$-micellar transition as measured by DSC for the acrylate system compared to the chloride system, indicating a better hydration of the system.

Conclusions

The phase behaviour of a novel polymerizable lyotropic ionic liquid crystal, C_{16}mimAcr, as a function of water has been investigated and compared to the chloride analogue, C_{16}mimCl. The C_{16}mimAcr system exhibits a more complex phase behaviour at 20 °C compared to the C_{16}mimCl, with the formation of a lamellar phase (L_α), a hexagonal phase (H_1) and a discontinuous cubic phase (I_1). On the other hand only the formation of a lamellar phase is observed for the C_{16}mimCl. The differences observed here for the two systems is likely due to the strong hydrating nature of the acrylate anion, which by increasing the head group area favours the formation of the additional lyotropic liquid crystalline mesophases. The polymerization facet of the C_{16}mimAcr system together with the additional formation of hexagonal phase (H_1) and discontinuous cubic phase (I_1) offers great potential in the conception of advanced nanostructured polymer with specific transport properties. Future work will investigate the UV-polymerizable properties of this system as well as the impact of crosslinking agent on mesophase present pre and post polymerization.

Acknowledgements

The authors are grateful to the Australian Research Council for funding this work through Australian Laureate Fellowship programs.

Notes and references

The terminology "smectic phase (SmA_2)" used in this manuscript refers to an interdigitated lamellar conformation.

1. J. J. Vallooran, S. Bolisetty and R. Mezzenga, *Advanced Materials*, 2011, 23, 3932-3937.
2. M. E. Tousley, X. Feng, M. Elimelech and C. O. Osuji, *ACS applied materials & interfaces*, 2014.
3. M. S. Mauter, M. Elimelech and C. O. Osuji, *Acs Nano*, 2010, 4, 6651-6658.
4. B. A. Pindzola, J. Jin and D. L. Gin, *Journal of the American Chemical Society*, 2003, 125, 2940-2949.
5. E. S. Hatakeyama, C. J. Gabriel, B. R. Wiesenauer, J. L. Lohr, M. Zhou, R. D. Noble and D. L. Gin, *Journal of Membrane Science*, 2011, 366, 62-72.
6. M. A. Firestone, J. A. Dzielawa, P. Zapol, L. A. Curtiss, S. Seifert and M. L. Dietz, *Langmuir*, 2002, 18, 7258-7260.
7. G. Zhang, X. Chen, Y. Zhao, Y. Xie and H. Qiu, *The Journal of Physical Chemistry B*, 2007, 111, 11708-11713.
8. X.-W. Li, J. Zhang, B. Dong, L.-Q. Zheng and C.-H. Tung, *Colloids and Surfaces A: Physicochemical and Engineering Aspects*, 2009, 335, 80-87.
9. R. Klein, G. J. Tiddy, E. Maurer, D. Touraud, J. Esquena, O. Tache and W. Kunz, *Soft Matter*, 2011, 7, 6973-6983.
10. F.-G. Wu, J.-S. Yu, S.-F. Sun and Z.-W. Yu, *Langmuir*, 2011, 27, 14740-14747.
11. K. Fontell, *Colloïd and polymer science*, 1990, 268, 264-285.
12. G. Lindblom and L. Rilfors, *Biochimica et Biophysica Acta (BBA)-Reviews on Biomembranes*, 1989, 988, 221-256.
13. R. Vargas, P. Mariani, A. Gulik and V. Luzzati, *Journal of molecular biology*, 1992, 225, 137-145.
14. Z. Wang, F. Liu, Y. Gao, W. Zhuang, L. Xu, B. Han, G. Li and G. Zhang, *Langmuir*, 2005, 21, 4931-4937.
15. Y. Huang, H. Cai, T. Yu, F. Zhang, F. Zhang, Y. Meng, D. Gu, Y. Wan, X. Sun and B. Tu, *Angewandte Chemie*, 2007, 119, 1107-1111.
16. R. Balmbra, J. Clunie and J. Goodman, 1969.
17. P. O. Eriksson, G. Lindblom and G. Arvidson, *Journal of Physical Chemistry*, 1987, 91, 846-853.
18. D. Batra, S. Seifert and M. A. Firestone, *Macromolecular Chemistry and Physics*, 2007, 208, 1416-1427.
19. T. Inoue, B. Dong and L.-Q. Zheng, *Journal of colloid and interface science*, 2007, 307, 578-581.
20. S. Sasaki, *The Journal of Physical Chemistry B*, 2007, 111, 2473-2476.
21. G. Zhang, X. Chen, Y. Xie, Y. Zhao and H. Qiu, *Journal of colloid and interface science*, 2007, 315, 601-606.
22. J. Zhang, B. Dong, L. Zheng, N. Li and X. Li, *Journal of colloid and interface science*, 2008, 321, 159-165.
23. C. Li, J. He, J. Liu, Z. Yu, Q. Zhang, C. He and W. Hong, *Journal of colloid and interface science*, 2010, 342, 354-360.
24. N. Byrne, D. Menzies, N. Goujon and M. Forsyth, *Chem. Commun.*, 2013.
25. D. L. Gin, W. Gu, B. A. Pindzola and W.-J. Zhou, *Accounts of chemical research*, 2001, 34, 973-980.
26. F.-G. Wu, N.-N. Wang, Q.-G. Zhang, S.-F. Sun and Z.-W. Yu, *Journal of colloid and interface science*, 2012, 374, 197-205.
27. M. A. DePierro and C. A. Guymon, *Macromolecules*, 2014, 47, 5728-5738.
28. J. D. Clapper and C. A. Guymon, *Macromolecules*, 2007, 40, 1101-1107.
29. J. D. Clapper, S. L. Iverson and C. A. Guymon, *Biomacromolecules*, 2007, 8, 2104-2111.
30. J. Zhang, Z. Xie, A. J. Hill, F. H. She, A. W. Thornton, M. Hoang and L. X. Kong, *Soft Matter*, 2012, 8, 2087-2094.
31. D. Batra, S. Seifert, L. M. Varela, A. C. Liu and M. A. Firestone, *Advanced Functional Materials*, 2007, 17, 1279-1287.
32. S. Grubjesic, S. n. Seifert and M. A. Firestone, *Macromolecules*, 2009, 42, 5461-5470.
33. M. Zhou, P. R. Nemade, X. Lu, X. Zeng, E. S. Hatakeyama, R. D. Noble and D. L. Gin, *Journal of the American Chemical Society*, 2007, 129, 9574-9575.
34. G. A. Becht, M. Sofos, S. n. Seifert and M. A. Firestone, *Macromolecules*, 2011, 44, 1421-1428.
35. A. Bradley, C. Hardacre, J. Holbrey, S. Johnston, S. McMath and M. Nieuwenhuyzen, *Chemistry of materials*, 2002, 14, 629-635.
36. A. Downard, M. Earle, C. Hardacre, S. McMath, M. Nieuwenhuyzen and S. Teat, *Chemistry of materials*, 2004, 16, 43-48.
37. F.-G. Wu, Q. Jia, R.-G. Wu and Z.-W. Yu, *The Journal of Physical Chemistry B*, 2011, 115, 8559-8568.
38. X. Zeng, Y. Liu and M. Impéror-Clerc, *The Journal of Physical Chemistry B*, 2007, 111, 5174-5179.
39. G. C. Shearman, A. I. Tyler, N. J. Brooks, R. H. Templer, O. Ces, R. V. Law and J. M. Seddon, *Journal of the American Chemical Society*, 2009, 131, 1678-1679.
40. J. Charvolin and J. Sadoc, *The Journal of Physical Chemistry*, 1988, 92, 5787-5792.
41. H. Delacroix, T. Gulik-Krzywicki, P. Mariani and V. Luzzati, *Journal of molecular biology*, 1993, 229, 526-539.
42. J. Wu, J. Zhang, L. Zheng, X. Zhao, N. Li and B. Dong, *Colloids and Surfaces A: Physicochemical and Engineering Aspects*, 2009, 336, 18-22.
43. A. Klaus, G. J. Tiddy, D. Touraud, A. Schramm, G. Stühler and W. Kunz, *Langmuir*, 2010, 26, 16871-16883.
44. C. K. Liu and G. G. Warr, *Soft matter*, 2014, 10, 83-87.
45. B. Wu, Y. Liu, Y. Zhang and H. Wang, *Chemistry-A European Journal*, 2009, 15, 6889-6893.
46. W. Jiang, Y. Wang and G. A. Voth, *The Journal of Physical Chemistry B*, 2007, 111, 4812-4818.
47. A. Mele, C. D. Tran and S. H. De Paoli Lacerda, *Angewandte Chemie*, 2003, 115, 4500-4502.
48. N. Goujon, N. Byrne, T. R. Walsh and M. Forsyth, *Australian Journal of Chemistry*, 2014.
49. C. A. Hall, K. A. Le, C. Rudaz, A. Radhi, C. S. Lovell, R. A. Damion, T. Budtova and M. E. Ries, *The Journal of Physical Chemistry B*, 2012, 116, 12810-12818.

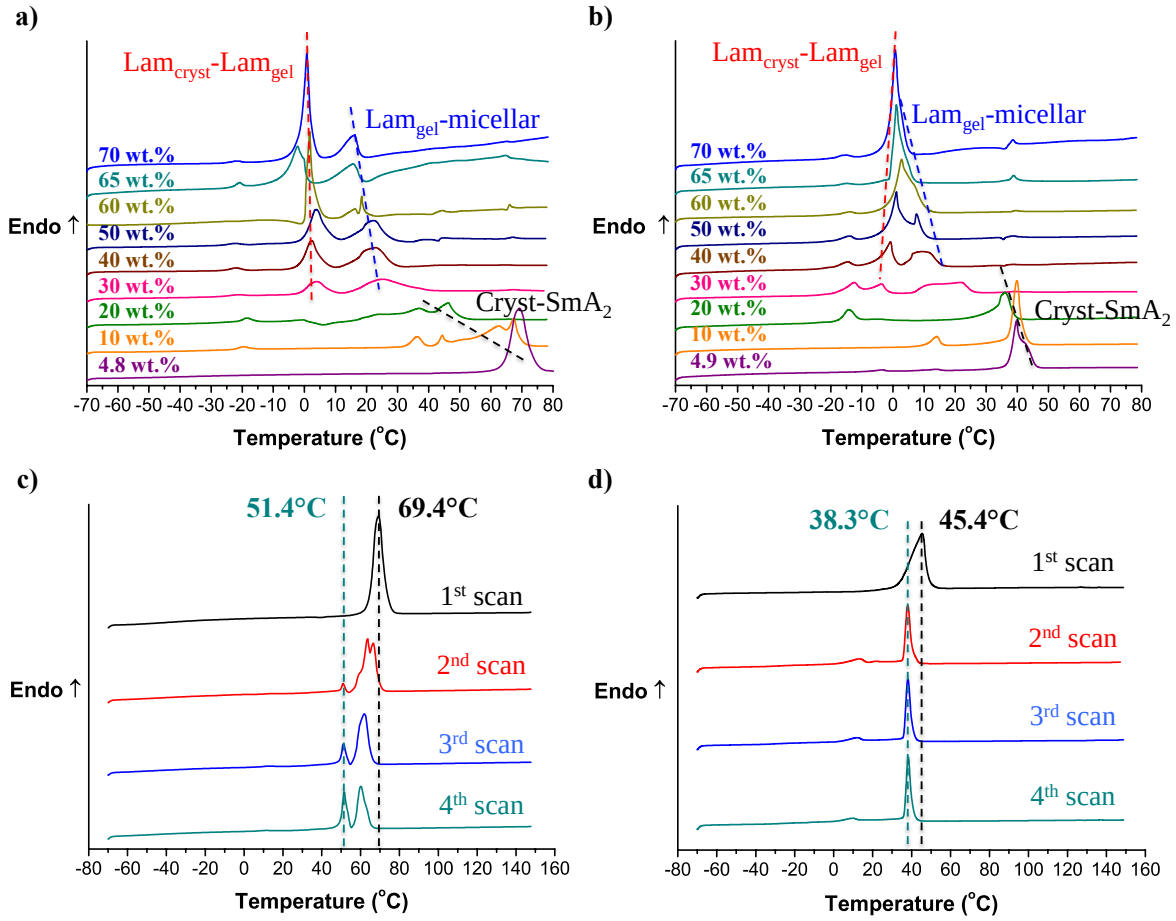

Figure 1: DSC heating profiles of the C_{16}mimCl (a) and C_{16}mimAcr (b) as a function of increasing water content (bottom to top), 4.8 or 4.9, 10, 20, 30, 40, 50, 60, 65 and 70 wt.% water. Repeated Scans of the C_{16}mimCl at 4.8 wt.% water (c) and C_{16}mimAcr at 4.9 wt.% water (d): 1st scan (black), 2nd scan (red), 3rd scan (blue) and 4thscan (cyan). (From -70 °C to 150 °C, 10 °C/min heating rate, 10 °C/min cooling rate).

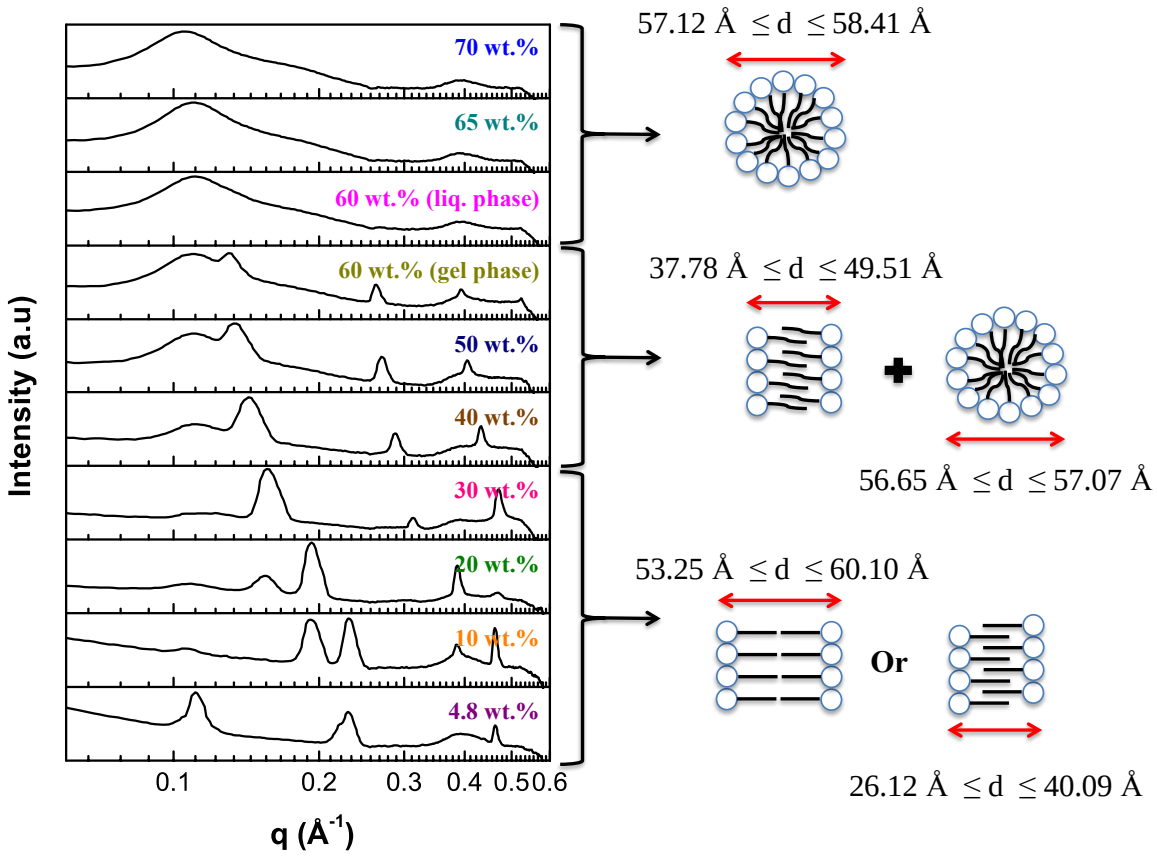

Figure 2: SAXS integrated patterns of the C_{16}mimCl as a function of water content as well as the schematic representation of the phase present. Blue sphere represents the imidazolium ring, anion and the water molecules, while black line represents the alkyl chain. The symbol "+" indicates the coexistence of two phases. While "or" implies one phase or the other.

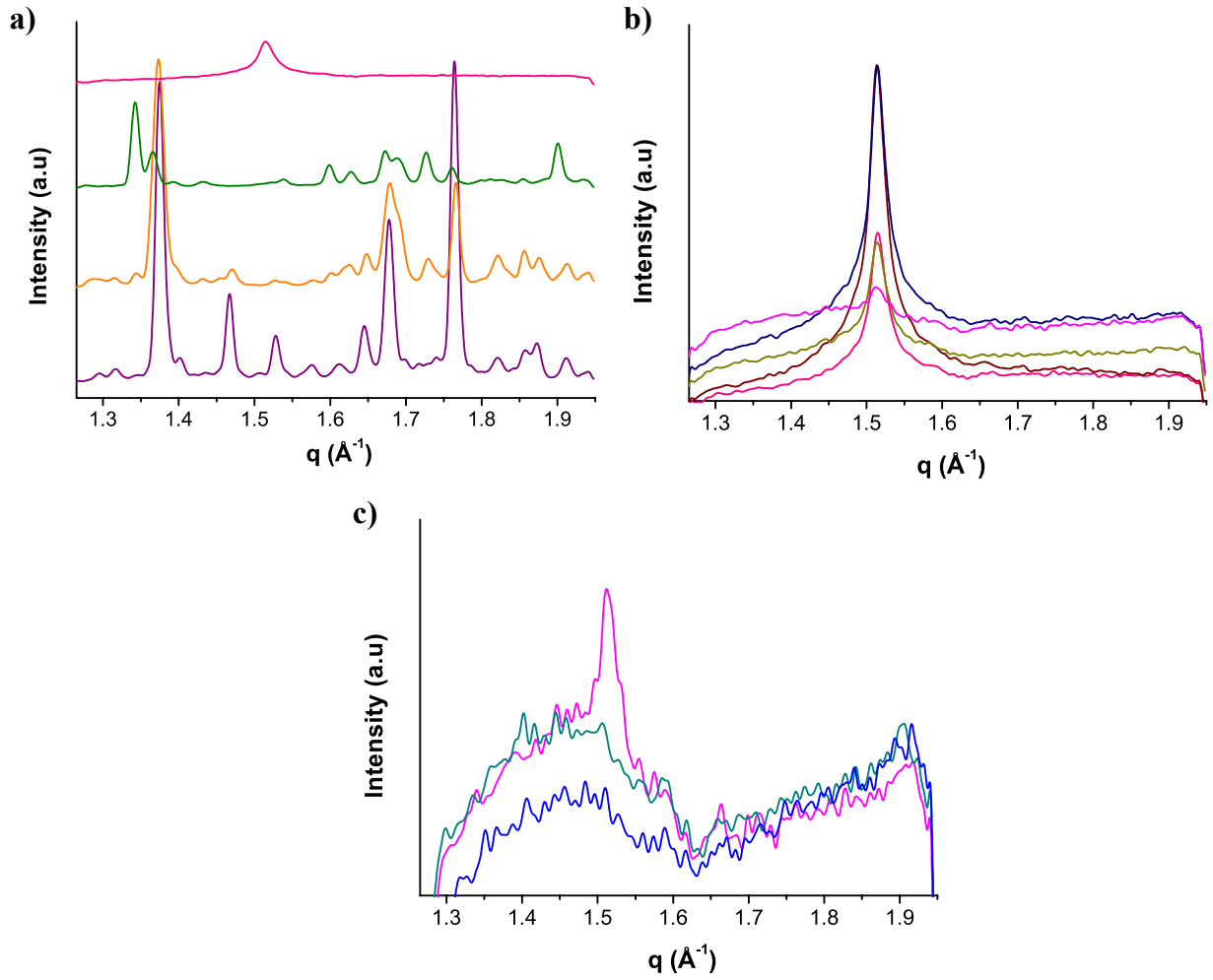

Figure 3: WAXS integrated patterns of the C_{16}mimCl as a function of water content: 4.8, 10, 20, 30 wt.%water (a) 30, 40, 50, 60 (gel), 60 (liq) wt.% water (b), 60 (liq), 65 and 70 wt.% water (c).

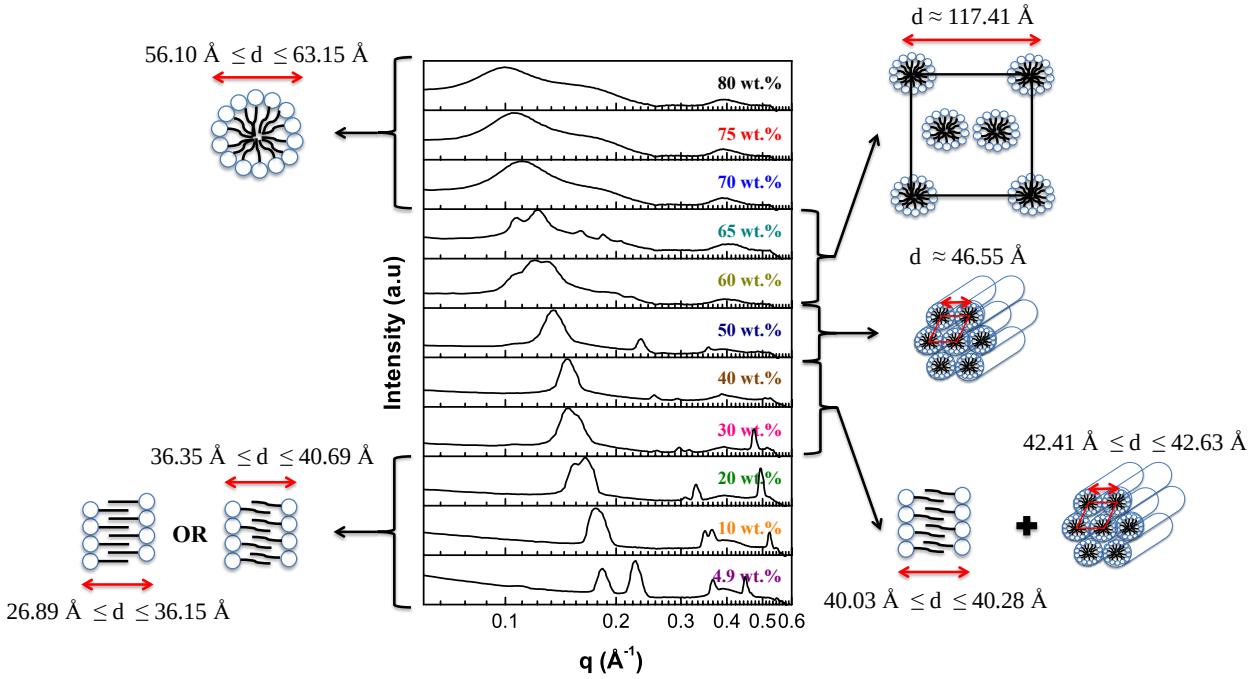

Figure 4: SAXS integrated patterns of the C_{16}mimAcr as a function of water content as well as the schematic representation of the phase present. Blue sphere represents the imidazolium ring, anion and the water molecules, while black line represents the alkyl chain. For the discontinuous cubic phase (I_1) only one face of the cubic unit cell is represented for clarity. The symbol "+" indicates the coexistence of two phases. While "or" implies one phase or the other.

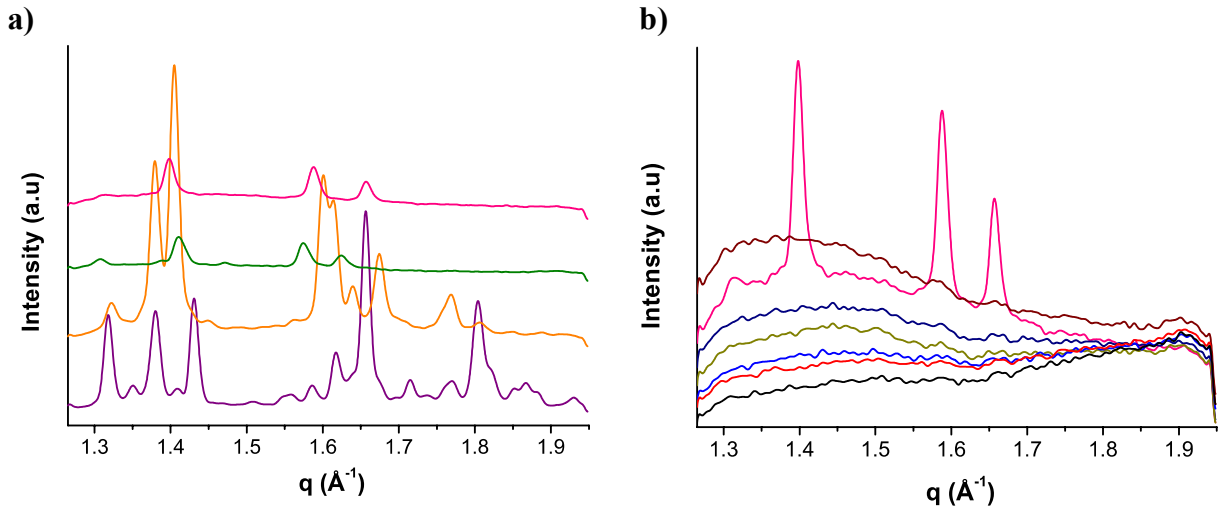

Figure 5: WAXS integrated patterns of the C_{16}mimAcr as a function of water content: 4.9, 10, 20, 30 wt.% water (a) 30, 40, 50, 60, 70, 75 and 80 wt.% water (b).

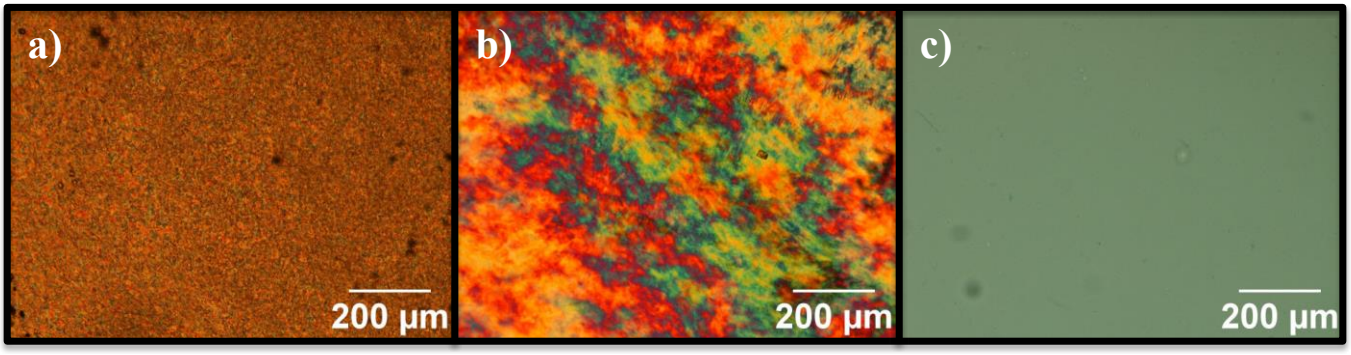

Figure 6: POM images of C_{16}mimAcr at 20 wt.% water (a), 40 wt.% water (b) and 60 wt.% water (c) at room temperature.

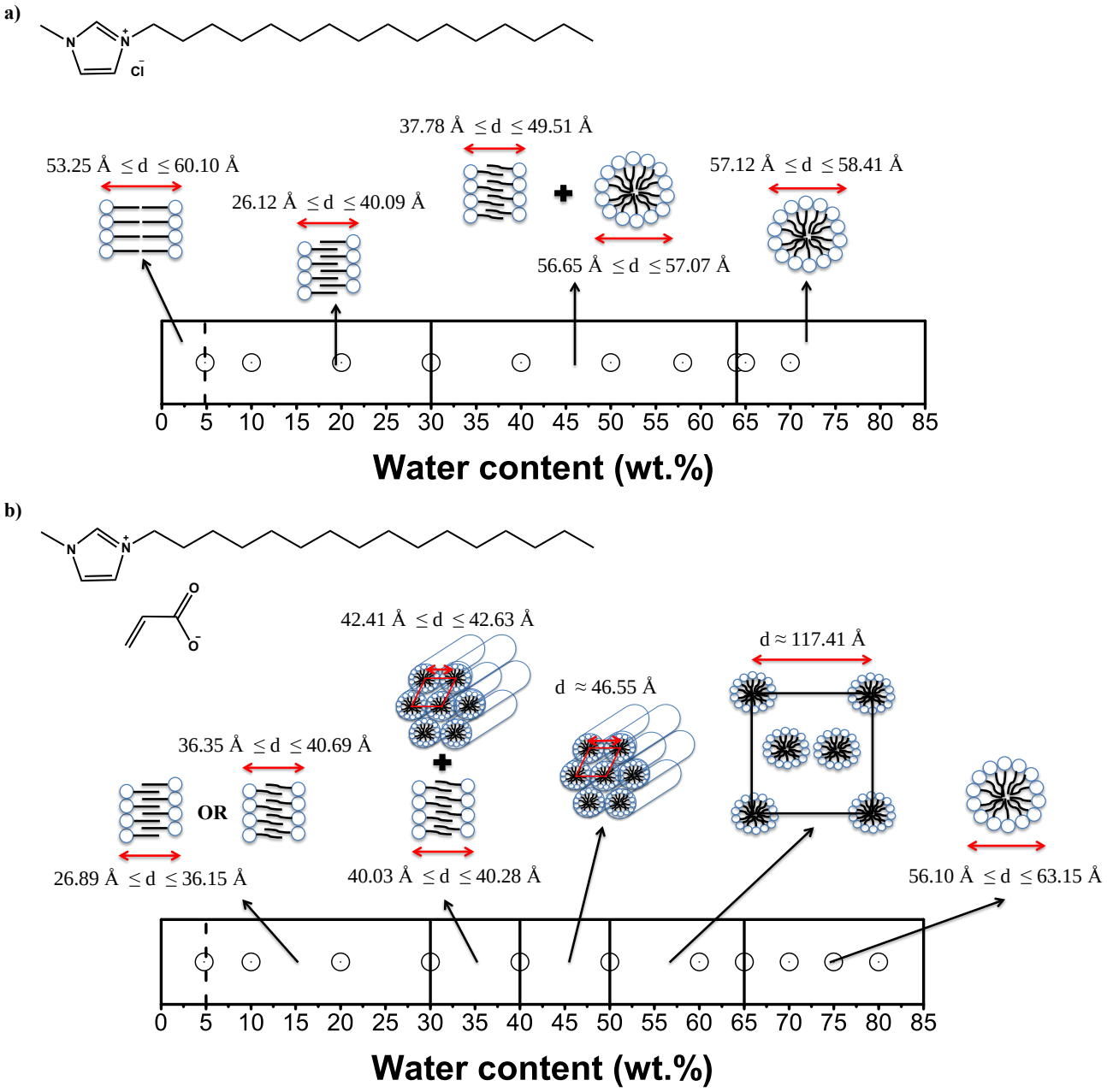

Figure 7 Phase diagram of the C_{16}mimCl (a) and the C_{16}mimAcr (b) as a function of water content at 20 °C established from the SAXS and WAXS data. Blue sphere represents the imidazolium ring, anion and the water molecules, while black line represents the alkyl chain. For the discontinuous cubic phase (I_1) only one face of the cubic unit cell is represented for clarity. The symbol "+" indicates the coexistence of two phases. While "or" implies one phase or the other.